Electronic Supplementary Material (ESI) for Nanoscale.

Supporting Information

Length feature of ssDNA adsorption onto graphene oxide with both large unoxidized and oxidized regions

Xiaoling Lei,[a‡] Huishu Ma,[b‡] Haiping Fang[a*]

[a] *Department of Physics, East China University of Science and Technology, Shanghai 200237, China*
[b] *Division of Interfacial Water and Key Laboratory of Interfacial Physics and Technology, Shanghai Institute of Applied Physics, Chinese Academy of Sciences, P.O. Box 800-204, Shanghai, 201800, China*

Contents

S1. Initial configurations for simulation with different length ssDNA molecules

The GO nanosheet was constructed based on the Shi-Tu structure model[1] with the formula of $C_{10}O_1(OH)_1(COOH)_{0.5}$ [2-4]. The size of the GO nanosheet was 10.084 nm × 10.224 nm in the *xz* plane (Fig. S1(f)), which contained 3936 carbon atoms, 311 hydroxyl groups (-OH) and 290 epoxy groups (-O-).The distribution of functional/oxidized groups on GO nanosheet was generated according to the rate-constant ratios based on the computation of both density functional theory and conventional transition-state theory. The oxidation loci on GO was highly correlated, in accordance with the recent experimental observations[5-12]. This high correlation led to the coexistence of both large unoxidized and oxidized regions on GO nanosheet with the correlation length of 4.2±0.5 nm. More importantly, on the oxidized regions of GO nanosheet, there were also some small areas of sp2-hybridized domains that we called 'island' region. Based on the correlations, the size of the patch islands was estimated to be up to 0.65±0.03 nm.

Initial configurations for simulation with different length ssDNA molecules were shown in Fig. S1. For short strand ssDNA, several ssDNA molecules were placed in one simulation system (four for 4 mer and two for 8 mer). For long strand ssDNA, each simulation system contained only one ssDNA molecule (one for 12mer, 16 mer and 20 mer). Details about these simulation systems were displayed in Table 1 in our Manuscript. Na atoms had been added to keep the simulation system charge-balanced. Meanwhile, oxidized region and unoxidized region on GO surface were separated by black curve as shown in Fig. S1(f).

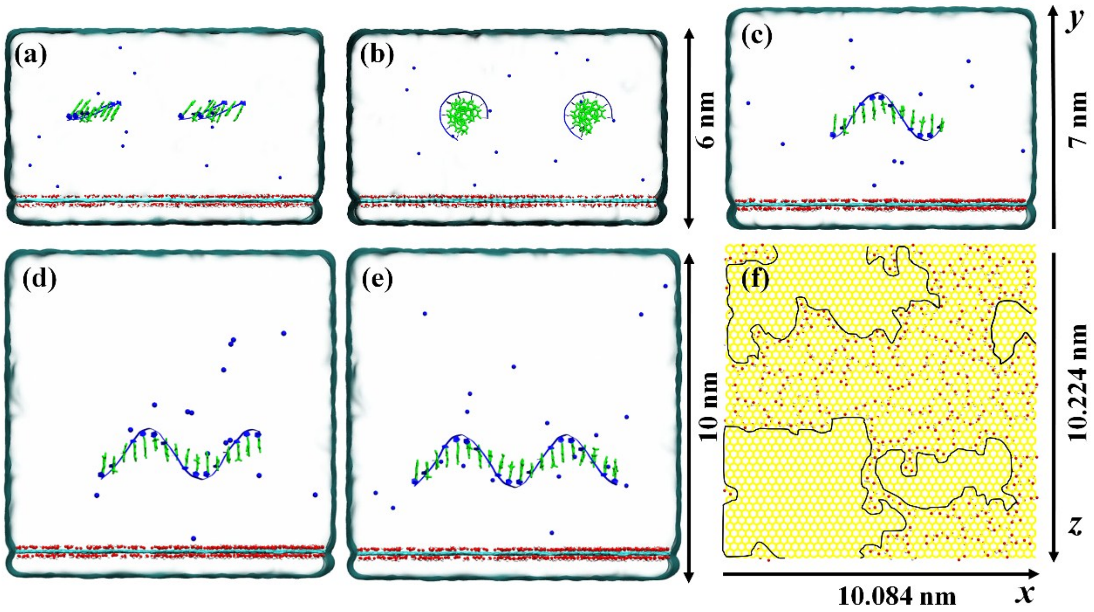

Fig. S1 Initial configurations for simulation with different length ssDNA molecules (a) 4 mer, (b) 8 mer, (c) 12 mer, (d) 16 mer, and (e) 20 mer embedded in water box adopting parallel orientation relative to the GO surface. Na atoms were represented by blue spheres. (f) Snapshot (top view) of the model GO surface. C, O and H atoms were represented by yellow, red and white spheres correspondingly. Oxidized region and unoxidized region on GO surface were separated by black curve.

S2. Adsorption configurations of different length ssDNA molecules

We present the final adsorption configurations of ssDNA molecules of 4 mer, 8 mer, 12 mer, 16 mer and 20 mer on GO surface. Even for the same length of ssDNA molecules, the final configurations of adsorbed ssDNA molecules differed from each simulation samples. For short strand ssDNA (from 4 to 8 mer), the ssDNA can adsorb completely not only on the oxidized or unoxidized region, but also on cross-border region between them, and the final configurations of adsorbed ssDNA were extended in most of the samples we simulated (Fig. S2(a) and (b)). However, for long strand ssDNA (from 12 to 20 mer), most ssDNA molecules were adsorbed on cross-border region, and we also found the existence of coiled structures of the final adsorbed ssDNA molecules, as shown in Fig. S2(c)~(e).

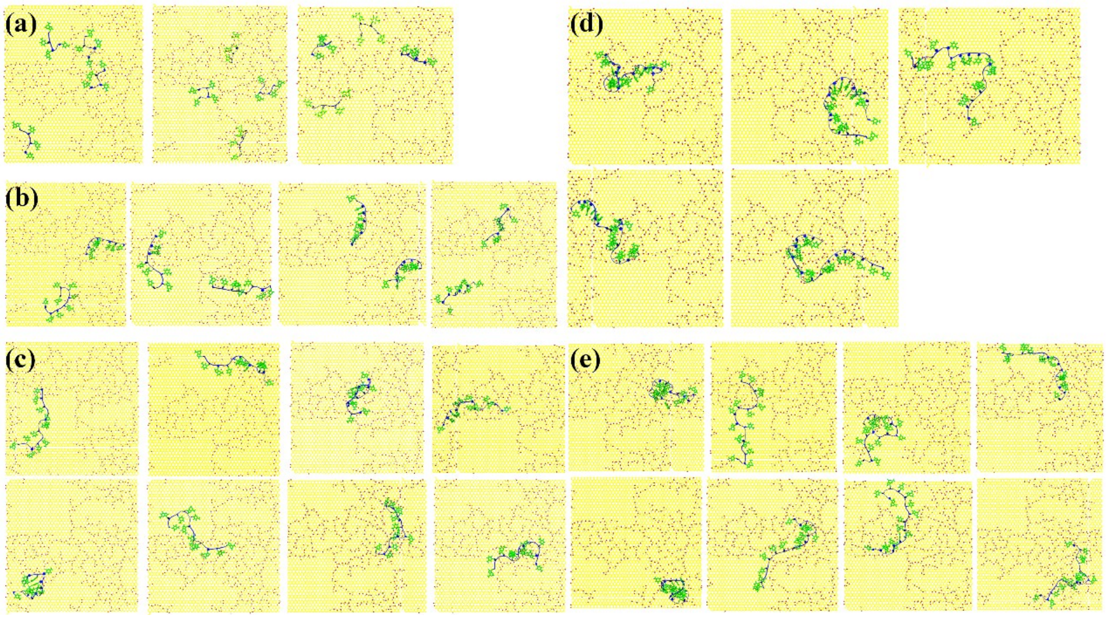

Fig. S2 Snapshots of the final adsorption configurations of different length ssDNA molecules (a) 4 mer, (b) 8 mer, (c) 12 mer, (d) 20 mer, and (e) 16 mer on GO surface.

S3. Dynamic adsorption of ssDNA molecules onto GO surface

To show the dynamic adsorption of ssDNA molecules onto GO surface, we calculated the center of mass (COM) distances in *y* axis and the interaction energy between GO surface and different length ssDNA molecules in Fig. S3(a) and Fig. S3(b). Initially, ssDNA was placed 3 nm above the GO surface, and they were completely noninteracting. However, as the simulations started, COM distance first undergoes some initial fluctuation, representing solvent-assisted free diffusion of the ssDNA. Thereafter, the distance gradually reduced and attained constancy, indicating the stepwise adsorption of ssDNA molecules onto GO surface. The interaction energy between ssDNA molecules and GO surface also had similar trends with the COM distance. In the last 100 ns of the simulation, the interaction energy fluctuated steadily, suggesting that the adsorption of ssDNA was in a dynamic equilibrium state. By comparing the adsorption process of different length ssDNA molecules onto GO surface, we found that, with the length increasing, the ssDNA molecules needed more time to start the adsorption process. Especially, for 16 mer, nearly half of the simulation systems needed a longer relaxation time to start the adsorption process, which was in accordance with the forming time of the π-π stacking structure between GO surface and ssDNA molecules. Carefully looking into the structure of 16 mer ssDNA, we found that nearly half of the 16 mer ssDNA molecules were self-folding in solution before they start the adsorption process (Fig. S3(c)).

Then, we also calculated the average number of hydrogen bonds (H-bonds) between different length ssDNA molecules and GO surface at last 20 ns, as shown in Fig. S3(d). From the result, we found that all ssDNA molecules could form more hydrogen bonds with the hydroxyl groups on the GO than that with the epoxy groups, which was in accordance with our previous results of the 12 mer ssDNA with random sequences on GO surface[13].

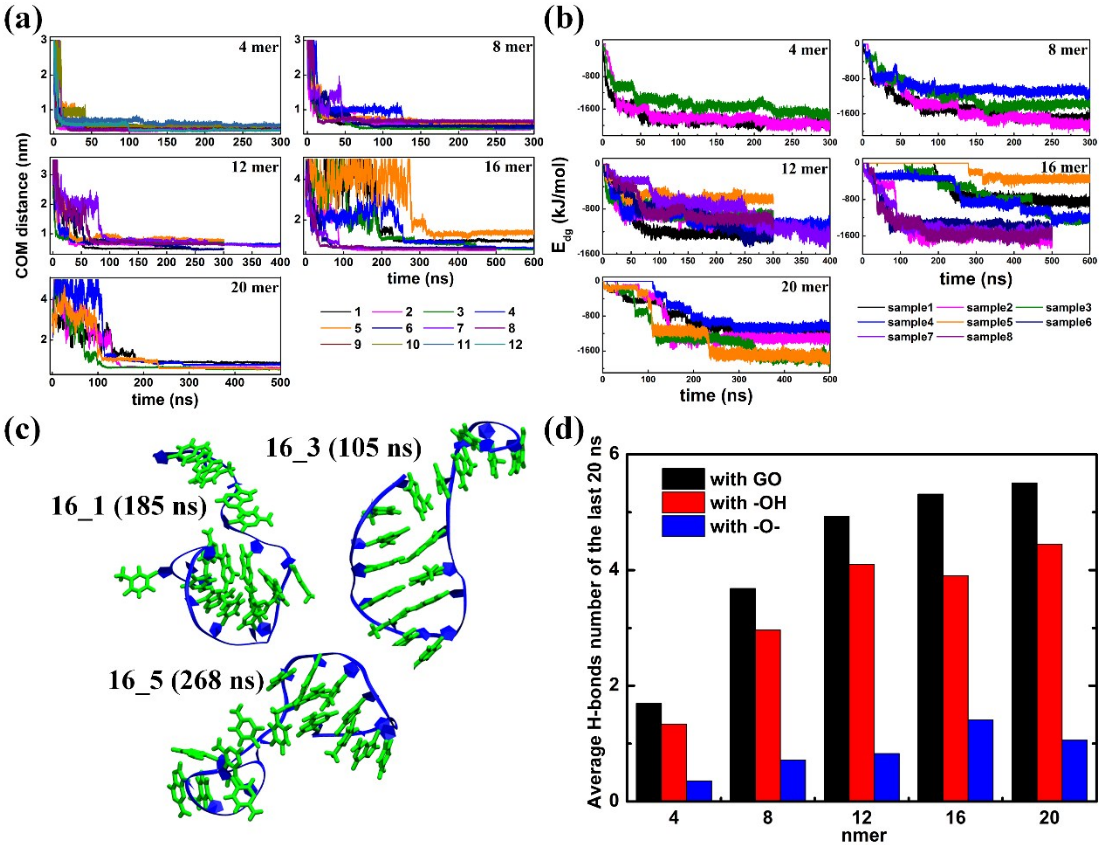

Fig. S3 Time evolution of (a) COM distances along the *y* axis and (b) interaction energy between GO surface and different length ssDNA molecules. Results from independent molecular dynamics (MD) samples were represented by different colors. (c) Typical snapshots of 16 mer ssDNA at given time for different simulation systems in solution. (d) Average number of hydrogen bonds formed between different length ssDNA molecules and GO (black bar), hydroxyl groups (red bar) and epoxy groups (blue bar) at last 20 ns.

S4. Distribution of nucleobases in the final adsorption configurations of ssDNA

To fully understand the feature of ssDNA adsorption on GO surface, we analyzed the distance and angle between nucleobases of ssDNA and GO surface at the final simulation time. With the length of ssDNA increasing, the range of distance and angle distribution also expanded, which meant that ssDNA contained more multilevel stack and nonstack structures in the long length ssDNA systems. The result was in accordance with the result shown in Fig. 1c. In this context, direct π stacking and other free structures might act as nucleation sites that enable rapid duplex formation and concomitant desorption of the duplex from the GO surface.

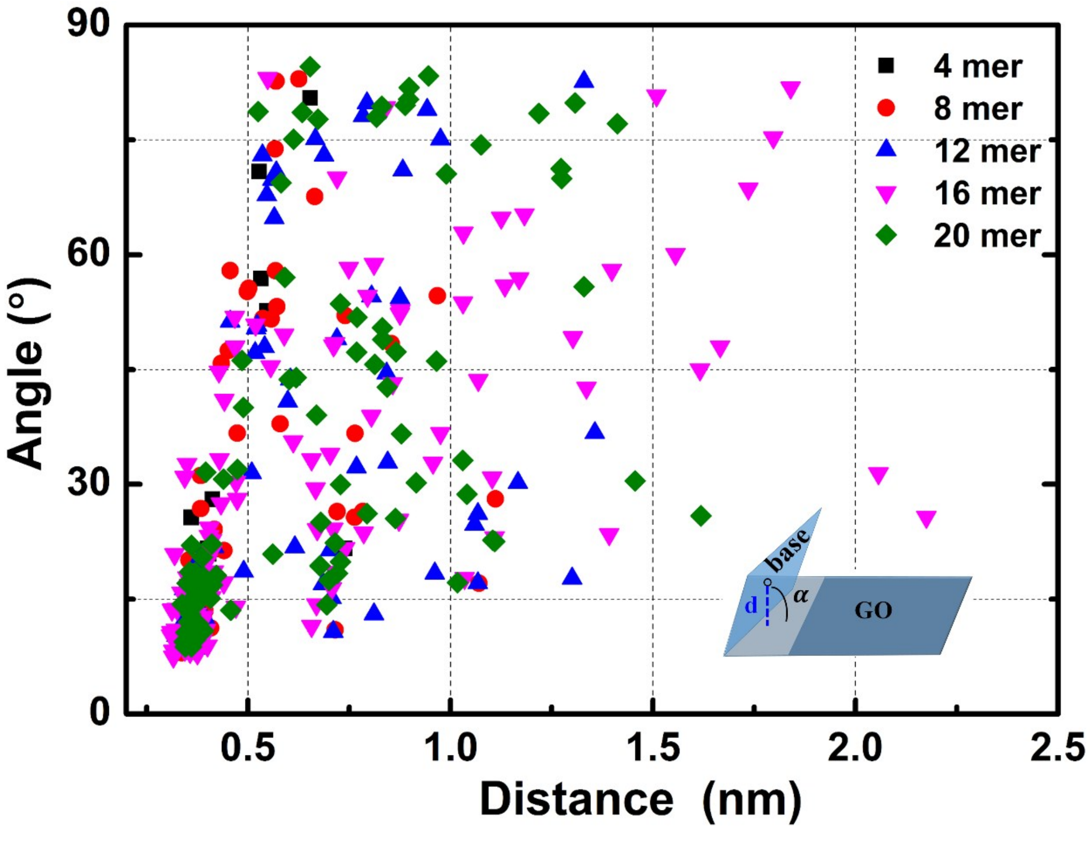

Fig. S4 Position of nucleobases of ssDNA relative to GO surface at the final simulation time for all simulations for different length ssDNA molecules (schematic of angle α and distance d are shown in insert map).

S5. Average lifetime of H-bond between water molecules and GO surface

A control system with GO surface embedded in water box was set to study the hydrogen bond (H-bond) between water and GO surface (Fig. S5(a)). MD simulation was performed with the NVT ensemble using GROMACS 4.5.4[14]. The temperature was maintained at 300 K using the v-rescale method. Periodic boundary conditions were imposed in the *xyz* directions. The time step in all simulations were set to 1 fs and the simulation data were collected every 5 fs. The Lennard–Jones (LJ) interactions were treated with a cutoff distance of 1.0 nm, and the particle mesh Ewald (PME) method[15] with a real-space cutoff of 1.0 nm was used for the long-range electrostatic interactions. The TIP3P model is utilized for the water molecules[16]. The detailed force field parameters of GO can be referred to Method of Manuscript.

As shown in Fig. S5(b), GO surface contained large unoxidized and oxidized regions, the boundary region was defined as the region which was centered on the oxygen atoms located at the junction area with the range of 0.35 nm[17], which was highlighted in dotted line. It is interesting to know the property of H-bond in boundary region. Fig. S5(c) shows the autocorrelation function $C_{H-bond}(t) = \frac{\langle h(0)h(t) \rangle}{\langle h(0)h(0) \rangle}$, where h(0)=1 indicates that water and oxidized group form a hydrogen bond initially, h(t)=1 means that water and oxidized group were still bonded at time *t*, and otherwise h(t)=0. We adopted a geometric definition of the hydrogen bond; namely, water molecules and oxidized groups are considered to be hydrogen bonded if their oxygen-oxygen distance is less than 3.5 Å, and the angle H-O…O is less than 30°[18]. By fitting the autocorrelation function with an exponential decay function $y_t = e^{-t/\tau_{H-bond}}$, we could obtain the lifetime $\tau_{H\text{-}bond}$ of the H-bond between water molecules and oxidized groups on GO surface[18-21]. The hydrogen bond lifetime between water molecules and oxidized groups located at the boundary regions was smaller than that located at the oxidized regions, corresponding to 9.46 ps and 9.92 ps respectively.

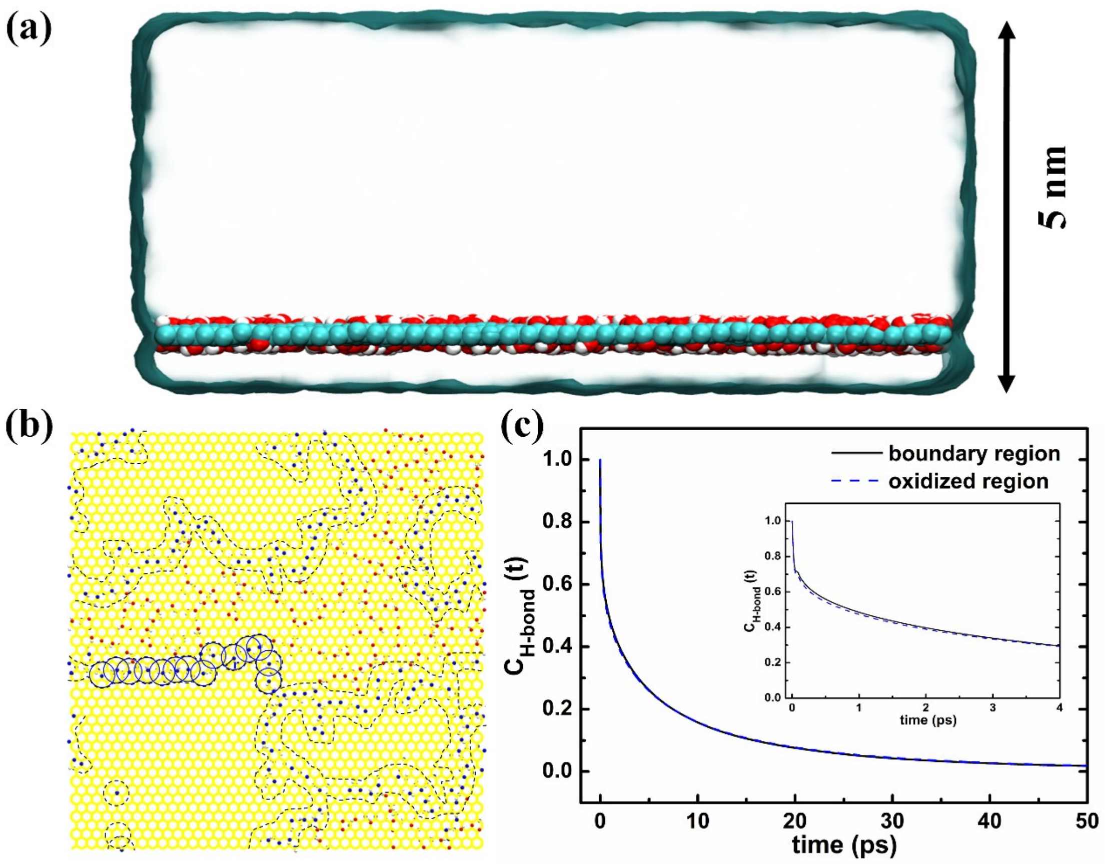

Fig. S5 (a) Initial configurations for simulation with GO surface embedded in water box. (b) Snapshot (top view) of the model GO sheet. C, O and H atoms were represented by yellow, red and white spheres correspondingly. Oxygen atoms at the junction of oxidized and unoxidized regions were highlighted in blue spheres. The boundary region was defined as the region which was centered on the oxygen atoms located at the junction area with the range of 0.35 nm, which was highlighted in dotted line. (c) Autocorrelation function *C*(*t*) of H-bond between water and oxidized groups (hydroxyl groups and epoxy groups) in boundary region or in oxidized region. In particular, the inserted figure showed the autocorrelation function of H-bond from 0 to 4 ps.

Reference

1. J. Yang, G. Shi, Y. Tu and H. Fang, *Angewandte Chemie International Edition*, 2014, **53**, 10190-10194.
2. A. Lerf, H. He, M. Forster and J. Klinowski, *The Journal of Physical Chemistry B*, 1998, **102**, 4477-4482.
3. N. V. Medhekar, A. Ramasubramaniam, R. S. Ruoff and V. B. Shenoy, *ACS nano*, 2010, **4**, 2300-2306.
4. C.-J. Shih, S. Lin, R. Sharma, M. S. Strano and D. Blankschtein, *Langmuir*, 2011, **28**, 235-241.
5. Y. Tu, M. Lv, P. Xiu, T. Huynh, M. Zhang, M. Castelli, Z. Liu, Q. Huang, C. Fan and H. Fang,

Nature nanotechnology, 2013, **8**, 594.

6. H. Geng, X. Liu, G. Shi, G. Bai, J. Ma, J. Chen, Z. Wu, Y. Song, H. Fang and J. Wang, *Angewandte Chemie International Edition*, 2017, **56**, 997-1001.
7. D. Chen, H. Feng and J. Li, *Chemical reviews*, 2012, **112**, 6027-6053.
8. D. R. Dreyer, S. Park, C. W. Bielawski and R. S. Ruoff, *Chemical society reviews*, 2010, **39**, 228-240.
9. W. Cai, R. D. Piner, F. J. Stadermann, S. Park, M. A. Shaibat, Y. Ishii, D. Yang, A. Velamakanni, S. J. An and M. Stoller, *Science*, 2008, **321**, 1815-1817.
10. J. C. Meyer, C. O. Girit, M. Crommie and A. Zettl, *Nature*, 2008, **454**, 319.
11. K. A. Mkhoyan, A. W. Contryman, J. Silcox, D. A. Stewart, G. Eda, C. Mattevi, S. Miller and M. Chhowalla, *Nano letters*, 2009, **9**, 1058-1063.
12. K. Erickson, R. Erni, Z. Lee, N. Alem, W. Gannett and A. Zettl, *Advanced Materials*, 2010, **22**, 4467-4472.
13. Z. Xu, X. Lei, Y. Tu, Z. J. Tan, B. Song and H. Fang, *Chemistry–A European Journal*, 2017, **23**, 13100-13104.
14. B. Hess, C. Kutzner, D. Van Der Spoel and E. Lindahl, *Journal of chemical theory and computation*, 2008, **4**, 435-447.
15. T. Darden, D. York and L. Pedersen, *The Journal of chemical physics*, 1993, **98**, 10089-10092.
16. W. L. Jorgensen, J. Chandrasekhar, J. D. Madura, R. W. Impey and M. L. Klein, *The Journal of chemical physics*, 1983, **79**, 926-935.
17. D. Xenides, B. R. Randolf and B. M. Rode, *Journal of Molecular Liquids*, 2006, **123**, 61-67.
18. C. Wang, H. Lu, Z. Wang, P. Xiu, B. Zhou, G. Zuo, R. Wan, J. Hu and H. Fang, *Physical Review Letters*, 2009, **103**, 137801.
19. Y. Guo and R. Wan, *Physical Chemistry Chemical Physics*, 2018, **20**, 12272-12277.
20. R. Wan, C. Wang, X. Lei, G. Zhou and H. Fang, *Physical review letters*, 2015, **115**, 195901.
21. J. Li, T. Liu, X. Li, L. Ye, H. Chen, H. Fang, Z. Wu and R. Zhou, *The Journal of Physical Chemistry B*, 2005, **109**, 13639-13648.